Cite this: *Mater. Horiz.*, 2016, 3, 328

The synthesis, structure and electronic properties of a lead-free hybrid inorganic–organic double perovskite $(MA)_2KBiCl_6$ (MA = methylammonium)†

Fengxia Wei,[a] Zeyu Deng,[a] Shijing Sun,[a] Fei Xie,[a] Gregor Kieslich,[a] Donald M. Evans,[b] Michael A. Carpenter,[b] Paul D. Bristowe[a] and Anthony K. Cheetham*[a]

In a search for lead-free materials that could be used as alternatives to the hybrid perovskites, $(MA)PbX_3$, in photovoltaic applications, we have discovered a hybrid double perovskite, $(MA)_2KBiCl_6$, which shows strong similarities to the lead analogues. Spectroscopic measurements and nanoindentation studies are combined with density functional calculations to reveal the properties of this interesting system.

Conceptual insights

Despite the stunning performance of methylammonium lead halides in thin film solar cells, the toxicity of lead will probably limit widespread adoption of the technology. We describe a new pathway towards lead-free alternatives in which Pb^{2+} is replaced by an environmentally benign combination of monovalent K^+ and trivalent Bi^{3+} to form a double perovskite. Our proof of concept system, the first hybrid inorganic–organic double perovskite, $(MA)_2KBiCl_6$, displays characteristics that are remarkably similar to the lead chloride hybrid perovskite, $(MA)PbCl_3$. In particular, $(MA)_2KBiCl_6$ adopts a perovskite architecture, is solution processable, and exhibits comparable mechanical properties to its lead chloride analogue. Our findings provide a new and viable route towards lead-free, hybrid semiconductors.

The light-harvesting, semiconducting hybrid inorganic–organic perovskites (HIOPs) have recently attracted a great deal of attention in the photovoltaic community, with their solar cell efficiencies rising from ~4% to over 20% in just six years.[1–3] The most extensively studied materials are the lead-containing systems, $APbX_3$, where A is an alkylammonium cation (*e.g.* $CH_3NH_3^+$ (methylammonium, MA) or $NH_2CHNH_2^+$ (formamidinium, FA)) and X is Cl^-, Br^- or I^-. However, the toxicity of lead to the environment could become a major drawback in their commercialisation and the quest for lead-free alternatives is therefore attracting a lot of attention. Other group IV metals such as Ge and Sn are being explored, but the chemical instability of Sn^{2+} and Ge^{2+} presents challenges for their practical utilisation.[4,5] Alternatively, the replacement of Pb^{2+} by isoelectronic ions also seems attractive because the strong light absorption and long carrier lifetimes exhibited by $MAPbX_3$ are believed to be related to the $6s^26p^0$ electronic configuration of Pb^{2+}.[6] While Tl^+ is also toxic, Bi^{3+} is an interesting option because coordination complexes of bismuth are used in over-the-counter medicines such as Pepto-Bismol.[7] However, this strategy poses challenges because Bi^{3+} has a different valence state from Pb^{2+} and cannot therefore be simply substituted into phases such as $(MA)PbX_3$. In the present work, we show that the incorporation of Bi^{3+} into a HIOP can be achieved by synthesising a hybrid double perovskite of general formula $(MA)_2M^IM^{III}X_6$.

There has been significant recent progress in the incorporation of Bi^{3+} into hybrid perovskite-related halides. For example, $(MA)_3Bi_2I_9$ can be readily obtained by using a synthetic route analogous to that used for $MAPbI_3$,[8] and an ammonium bismuth iodide phase, $(NH_4)_3Bi_2I_9$, was recently reported to show a bandgap of 2.04 eV.[9] A number of alkali metal systems of composition $M^I_3Bi_2I_9$ (M = K, Rb, Cs) have also been described.[10,11] None of these systems is a perovskite, however, and their structures have lower dimensionalities and therefore wider band gaps than their 3D analogues. In order to maintain the 3D perovskite architecture, an alternative approach is to use a combination of a monovalent cation, such as an alkali metal or Ag^+, and a trivalent cation such as Bi^{3+}, in an ordered B-site arrangement to form a double perovskite structure of general formula $A^I_2B^IB^{III}X_6$. During the 1970s, a number of double perovskites (which were described by their alternative name, elpasolites) of composition $Cs_2NaM^{III}Cl_6$ (M^{III} = lanthanide, actinide, bismuth, and so on) were reported in $Fm\bar{3}m$ symmetry, wherein the perovskite network contains alternating $NaCl_6$ and $M^{III}Cl_6$

[a] *Department of Materials Science and Metallurgy, University of Cambridge, 27 Charles Babbage Road, CB3 0FS, UK. E-mail: akc30@cam.ac.uk*
[b] *Department of Earth Sciences, University of Cambridge, Downing Street, CB2 3EQ, UK*

† Electronic supplementary information (ESI) available: Some DFT calculations and experimental details and results such as X-ray diffraction, TGA, nanoindentation, RUS. CCDC 1456389. For ESI and crystallographic data in CIF or other electronic format see DOI: 10.1039/c6mh00053c

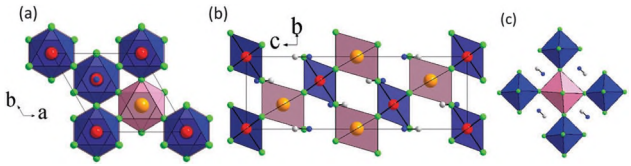

Fig. 1 Crystal structure of $(MA)_2KBiCl_6$, obtained from single crystal X-ray diffraction, viewed along (a) the *c* axis, (b) the *a* axis, and (c) tilted to show the MA location. Red: Bi, brown: K, green: Cl, white: C, blue: N. $BiCl_6$ and KCl_6 octahedra are shown in blue and purple, respectively.

octahedra on the B-sites.[12] At that time, particular interest focused on a ferroelectric phase transition that was observed on cooling $Cs_2NaBiCl_6$.[13–16] Very recently, and in the light of the intense interest in halide perovskites, McClure *et al.* reported Cs_2AgBiX_6 (X = Cl, Br) with a bandgap of 2.77 eV for X = Cl and 2.19 eV for X = Br,[17] while a separate paper by Slavney *et al.* described the X = Br phase with a bandgap of 1.95 eV and a long photoluminescence lifetime of *ca.* 660 ns.[18] The observation that hybrid perovskites are more easily processed into devices and show different optical properties compared with their inorganic analogues[19] encouraged us to investigate the possibility of making hybrid double perovskites. Here we report such a material, $(MA)_2KBiCl_6$, which crystallises in rhombohedral $R\bar{3}m$ symmetry and contains alternating KCl_6 and $BiCl_6$ octahedra that are corner-sharing to form a 3D network (Fig. 1). The experimentally observed structure is compared with density functional theory (DFT) calculations, and we also report the results of absorption spectroscopy, thermal analysis, resonant ultrasound spectroscopy (RUS) and nanoindentation measurements.

Synthesis: The starting material, CH_3NH_3Cl, was prepared by mixing stoichiometric amounts of methylamine solution (40 wt% in H_2O) and HCl (37% in H_2O) at 273 K, then heating at 333 K to dryness, washing with acetone, and drying overnight in a vacuum oven. Crystals of $(MA)_2KBiCl_6$ were synthesised at 423 K by the hydrothermal method in a stainless steel Parr autoclave using 2.4 mmol CH_3NH_3Cl, 1.2 mmol KCl and 1.2 mmol $BiCl_3$ in 1 ml HCl acid solution. Single phase powders can be obtained through solvent precipitation from hot HCl acid.

Thermogravimetric analysis (TGA) and differential scanning calorimetry (DSC) were conducted using an SDT (simultaneous DSC-TGA) Q600 instrument. 13.89 mg of powder sample was heated from room temperature to 1073 K at 10 K min^{-1} under a nitrogen flow of 100 ml min^{-1}. A peak was observed at *ca.* 333 K in the DSC curve, indicating a possible phase transition as there was no mass loss in the corresponding TGA curve (Fig. S1, ESI†). Samples started to decompose from *ca.* 503 K, which is near the MACl boiling range (498–503 K) and $BiCl_3$ melting point (500 K). Around 60% weight loss was observed at *ca.* 703 K, and the amount reached ~77% at *ca.* 836 K.

$(MA)_2KBiCl_6$ crystallises in $R\bar{3}m$ symmetry (CCDC 1456389), with lattice parameters a = 7.8372(2) Å and c = 20.9938(7) Å. Alternating KCl_6 and $BiCl_6$ octahedra share corners to form an ReO_3-like framework and the MA cations occupy the A-site cavities to complete the double perovskite structure. We estimate that $(MA)_2KBiCl_6$ has a tolerance factor of 0.93, which is well within the range (0.80–1.0) where the perovskite structure can be expected to form.[20] Due to the obvious size difference between the radii of K^+ (1.38 Å) and Bi^{3+} (1.03 Å),[21] the 3D network is distorted from the cubic stacking that is seen in caesium-based Na/Bi and Ag/Bi double perovskites. The KCl_6 octahedra are slightly distorted with K–Cl bond lengths of 3.049(2) Å and two octahedral bond angles of 81.67(9)° and 98.33(9)°, while the $BiCl_6$ octahedra are more regular in shape with Bi-Cl distances of 2.681(2) Å and bond angles of 91.76(10)° and 88.24(10)° (Tables S3 and S4, ESI†). The bridging angle between the KCl_6 and $BiCl_6$ octahedra is slightly bent with a K–Cl–Bi angle of 173.04(12)°. The structure is less tilted than the low-temperature orthorhombic form of $(MA)PbCl_3$, where the Pb–Cl–Pb bond angles range from 154.88(11) to 169.46(4)°.[22]

The MA cations in the perovskite A-site are aligned along the *c* direction (Fig. 1c) and alternate; symmetry-equivalent MA cations adopt opposite orientations (C–N···N–C) and have C–N bond lengths of 1.35(3) Å. The X-ray measurements are unable to locate the hydrogen atoms, so we cannot be sure whether the MA cations are ordered (which is allowed in space group $R\bar{3}m$), or disordered. However, hydrogen bonding is implied between the amine and the chloride anion since the N···Cl distance (3.406(1) Å) is shorter than the C···Cl one (3.848(2) Å). The corresponding distances for N···Cl in orthorhombic $(MA)PbCl_3$ are 3.273(2) Å, 3.346(2) Å, 3.366(10) Å and 3.421(2) Å,[22] suggesting that hydrogen bonding is important for both structures. Strong anisotropic atomic displacement parameters for the Cl anions indicate a possible rotational/tilting feature for the octahedra (Fig. S3, ESI†), which may be associated with MA cation disorder.

The lattice parameters obtained from powder X-ray diffraction are in good agreement with those obtained from single crystal X-ray diffraction. No secondary phase was detected for products synthesised by both solution precipitation and hydrothermal methods (Fig. S2, ESI†).

The optical bandgap was estimated using UV-visible spectrometry. The reflectance spectrum shows two edges and values of 3.04 eV and 3.37 eV were obtained for the apparent optical bandgaps from the corresponding Tauc plot (Fig. 2). The DFT calculations (below) have allowed us to interpret these observations.

Nanoindentation was carried out normal to the (001) plane of the single crystals. The Young's modulus was found to be

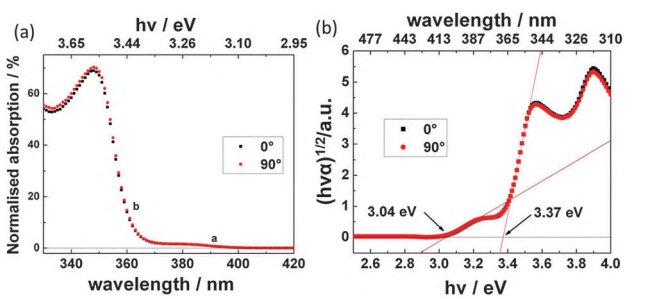

Fig. 2 (a) Normalised absorption spectra converted from reflectance data and (b) the Tauc plot (assumed indirect bandgap).

10.50 ± 1.18 GPa and the hardness 0.39 ± 0.07 GPa, averaging the results from an indentation depth of 200 nm to 900 nm (See Fig. S5 and S6, ESI†). In comparison with the experimental mechanical properties of the lead-based perovskites, the Young's modulus of $(MA)_2KBiCl_6$ is comparable with that of $(MA)PbI_3$ ($E \approx 11$ GPa) and lower than that of $(MA)PbCl_3$ ($E \approx 17$–20 GPa).[23] Since the crystal structures of $(MA)PbCl_3$ and $(MA)_2KBiCl_6$ adopt the same topology and differ only in terms of the B-site cations, the greater compliance of $(MA)_2KBiCl_6$ can be attributed to the weaker K–Cl bonding in comparison with that of Pb–Cl. Similar mechanical behaviour has been observed in previous work. For example, replacing Zn^{2+} cations with alternating Li^+ and B^{3+} in zeolitic imidazolate frameworks (ZIFs) reduces the elastic modulus from 8–9 GPa for $Zn(Im)_2$ to ~3 GPa for $LiB(Im)_4$.[24]

DFT geometry optimisation in $R\bar{3}m$ results in lattice parameters of a = 7.8165 Å and c = 20.9904 Å, which agree well with the single crystal XRD measurements. The DFT methods were used to predict the locations of the hydrogen atoms which could not be determined using X-rays (though they could in principle be obtained using neutron diffraction[25]). Note that since the space group could be consistent with both ordered or disordered hydrogen positions, the calculations do not establish whether the system is ordered at room temperature. Tables S1, S3 and S4 (ESI†) compare the fractional atomic coordinates, bond lengths and bond angles obtained from the calculations with those from the X-ray measurements; again it is seen that the agreement is very good. The maximum deviation is in the C–N bond distance (1.492 Å *vs.* 1.35(3) Å), which is a possible indication of MA disorder in the experimental structure.

Fig. 3(a and b) shows the calculated band structure of $(MA)_2KBiCl_6$, which predicts an indirect band gap of 3.02 eV, in good agreement with our optical measurements (3.04 eV). We postulate that such good agreement is probably due to the weaker spin–orbit coupling effect on K. Note that a direct transition would also be possible at 3.15 eV, which is consistent with the experimental feature at 3.37 eV (see above). The corresponding total and partial electronic density of states (Fig. S7(a), ESI†) reveal that MA does not contribute to states near the valence band maximum (VBM) or the conduction band minimum (CBM), which is similar to the case for $(MA)PbI_3$.[26] It is seen that Bi and Cl are the main contributors to states near the band gap. This can be further visualised in real space (Fig. S7(b), ESI†) by calculating the band decomposed partial charge density (PCD). It is seen that the valence band edge is composed of Bi-6s and Cl-3p antibonding states whereas the conduction band edge is composed of Bi-6p, Cl-3p antibonding states together with a small contribution from Cl-3s. However, the energy states of K are low lying; *e.g.* the K-3p states (not shown in the figure) occur at ~13 eV below the VBM. This differs from $Cs_2AgBiBr_6$[17] where Ag contributes energy states near the valence band edge.

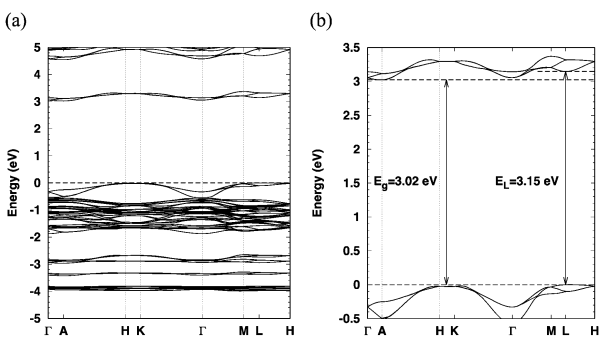

Fig. 3 (a) Calculated band structure of $(MA)_2KBiCl_6$ (b) enlarged view of the band structure near the band gap. The following high symmetry points in the first Brillouin zone were used: Γ (0, 0, 0), A (0, 0, 0.5), H (−0.333, 0.667, 0.5), K (−0.333, 0.667, 0), M (0, 0.5, 0) and L (0, 0.5, 0.5). The band edges are found at L in the valence band and A in the conduction band.

Single crystal stiffness constants (C_{ij}) were calculated from the stress–strain relationship by applying 2 types of strain: e_1 and $e_3 + e_4$ to the cell (each strain with ±0.5% and ±1% deformation) and relaxing the internal degrees of freedom.[27] A tensorial analysis[28] of the stiffness constants reveals the whole elastic anisotropy of $(MA)_2KBiCl_6$ (Table S6, ESI†). In order to better understand the mechanical properties of $(MA)_2KBiCl_6$, the directional Young's modulus in 3D is calculated and shown in Fig. S9 (ESI†) together with contour sections on three different planes. It is easy to see that the directions along Bi–Cl–K bonds have the largest value of the Young's modulus, which is very similar to $(MA)PbX_3$ (X = Cl, Br and I).[23] The calculations predict a Young's modulus of 15.28 GPa normal to the (001) facet, which is in reasonable agreement with the experimental nanoindentation results.

Resonant ultrasound spectroscopy (RUS) provides a highly sensitive method for detecting phase transitions through the influence of strain coupling effects.[29] The spectra reported here were obtained using electronics designed by Dr A. Migliori in Los Alamos, with a maximum applied voltage of 2 V, and a sample holder described by McKnight *et al.*[30] which was lowered into an Oxford Instruments Teslatron cryostat. Each spectrum contained 135 000 data points in the frequency range 0.01–1 MHz collected from an irregular shaped crystal (maximum dimensions ~1.5–2 mm and mass 0.0012 g) during a sequence of cooling and heating between 307 K and 1.5 K in 5 K steps. The sample chamber had first been evacuated and then filled with a few mbars of helium as exchange gas. A 10 minute settle time before data collection was allowed at each set point to allow thermal equilibration.

Fig. 4 shows segments of the spectra stacked in proportion to the temperature at which they were collected. Four features are immediately apparent (i) there is a break in trend and peak widths at ~260 K; (ii) there is then a clear hysteresis between cooling and heating through the interval ~125–260 K; (iii) the trend with reducing temperature for most resonances is of elastic softening below ~170 K, and (iv) individual resonances weaken or disappear in the vicinity of 50 K but reappear at the lowest temperatures. Selected peaks were fitted with an asymmetric Lorentzian function to follow their frequency, f, and width at half maximum height, Δf. Values of the elastic constants, which determine each resonant mode, scale with f^2, and the inverse mechanical quality factor, given by $Q^{-1} = \Delta f/f$, is a measure of acoustic attenuation. Data from peaks with

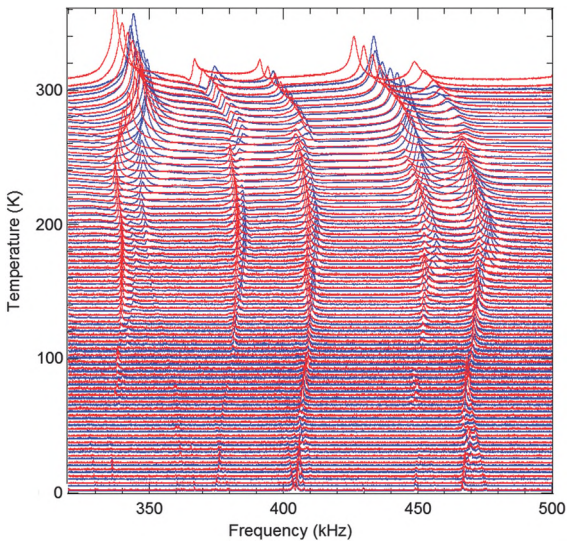

Fig. 4 Segments of RUS spectra collected during cooling (blue) and heating (red). The *y*-axis is the amplitude in volts from the detecting transducer, but the spectra have been offset in proportion to the temperature at which they were collected and the axis labelled as temperature.

resonance frequencies ~400 and ~460 kHz at room temperature are shown in Fig. S10 (ESI†). Stepwise softening immediately below ~265 K, accompanied by a peak in Q^{-1}, is similar to that seen at the octahedral tilting transition in $EuTiO_3$,[31] except that there is a hysteresis in the position of the anomaly between heating (267 K) and cooling (260 K). In comparison with $EuTiO_3$, the magnitude of the softening is small but the overall pattern is characteristic of a first order phase transition with weak coupling of strain to the driving order parameter. The softening trend with cooling below ~150 K is indicative of another incipient instability, as seen also in $LaAlO_3$,[32] and the near disappearance of resonance peaks in the interval ~30–60 K is suggestive of some additional process with weak strain coupling.

In conclusion, we have discovered a lead-free, hybrid double perovskite, $(MA)_2KBiCl_6$, which shows strong similarities to the widely-studied lead halide perovskites $(MA)PbX_3$. The system has a wide band gap of 3.04 eV, which is similar to that of the compound $(MA)PbCl_3$ (~3.0 eV).[33] Resonant ultrasound spectroscopy points to a series of phase transitions that may be associated with hydrogen bond ordering or octahedral tilting transitions, or both. Our findings also suggest that many other compositions should be explored with a view to making a lead-free, semiconducting analogue of $(MA)PbI_3$; these include $(MA)_2CuBiI_6$, $(MA)_2AgBiI_6$, and $(MA)_2TlBiI_6$ (we note that the latter compound has been the subject of a recent DFT study[34]). Our preliminary investigations suggest that bromide and iodide analogues require different synthesis conditions compared with the chlorides. Further experimental work along these lines is currently underway in our laboratory.

Acknowledgements

F. Wei is a holder of an A*STAR international fellowship granted by the Agency for Science, Technology and Research, Singapore. G. Kieslich and A. K. Cheetham thank the Ras al Kaihmah Center for Advanced Materials for financial support. G. Kieslich further thanks the DFG for financial support (KI1870). S. Sun and Z. Deng would like to thank the Cambridge Overseas Trust and the China Scholarship Council. The calculations were performed at the Cambridge HPCS and the UK National Supercomputing Service, ARCHER. Access to the latter was obtained *via* the UKCP consortium and funded by EPSRC under Grant No. EP/K014560/1. All necessary computational data is included in the manuscript or ESI.† RUS facilities were established in Cambridge through grants to MAC from the Natural Environment Research Council (NE/B505738/1, NE/F017081/1) and the Engineering and Physical Sciences Research Council (EP/I036079/1).

Notes and references

1 A. Kojima, K. Teshima, Y. Shirai and T. Miyasaka, *J. Am. Chem. Soc.*, 2009, **131**, 6050–6051.
2 M. M. Lee, J. Teuscher, T. Miyasaka, T. N. Murakami and H. J. Snaith, *Science*, 2012, **338**, 643–647.
3 National Renewable Energy Labs (NREL) Efficiency Chart. http://www.nrel.gov/ncpv/images/efficiency_chart.jpg, (accessed, 01-03, 2016).
4 N. K. Noel, S. D. Stranks, A. Abate, C. Wehrenfennig, S. Guarnera, A.-A. Haghighirad, A. Sadhanala, G. E. Eperon, S. K. Pathak, M. B. Johnston, A. Petrozza, L. M. Herz and H. J. Snaith, *Energy Environ. Sci.*, 2014, **7**, 3061–3068.
5 C. C. Stoumpos, L. Frazer, D. J. Clark, Y. S. Kim, S. H. Rhim, A. J. Freeman, J. B. Ketterson, J. I. Jang and M. G. Kanatzidis, *J. Am. Chem. Soc.*, 2015, **137**, 6804–6819.
6 J. M. Frost, K. T. Butler, F. Brivio, C. H. Hendon, M. van Schilfgaarde and A. Walsh, *Nano Lett.*, 2014, **14**, 2584–2590.
7 L. A. Tillman, F. M. Drake, J. S. Dixon and J. R. Wood, *Aliment. Pharmacol. Ther.*, 1996, **10**, 459–467.
8 R. Jakubas, J. Zaleski and L. Sobczyk, *Ferroelectrics*, 1990, **108**, 109–114.
9 S. Sun, S. Tominaka, J.-H. Lee, F. Xie, P. D. Bristowe and A. K. Cheetham, *APL Mater.*, 2016, **3**, 031101.
10 B. Chabot and E. Parthe, *Acta Crystallogr., Sect. B: Struct. Crystallogr. Cryst. Chem.*, 1978, **34**, 645–648.
11 A. J. Lehner, D. H. Fabini, H. A. Evans, C.-A. Hébert, S. R. Smock, J. Hu, H. Wang, J. W. Zwanziger, M. L. Chabinyc and R. Seshadri, *Chem. Mater.*, 2015, **27**, 7137–7148.
12 L. R. Morss, M. Siegal, L. Stenger and N. Edelstein, *Inorg. Chem.*, 1970, **9**, 1771–1775.
13 F. Pelle, B. Blanzat and B. Chevalier, *Solid State Commun.*, 1984, **49**, 1089–1093.
14 W. M. A. Smit, G. J. Dirksen and D. J. Stufkens, *J. Phys. Chem. Solids*, 1990, **51**, 189–196.
15 I. N. Flerov, M. V. Gorev, K. S. Aleksandrov, A. Tressaud, J. Grannec and M. Couzi, *Mater. Sci. Eng., R*, 1998, **24**, 81–151.
16 F. Prokert and K. S. Aleksandrov, *Phys. Status Solidi B*, 1984, **124**, 503–513.
17 E. T. McClure, M. R. Ball, W. Windl and P. M. Woodward, *Chem. Mater.*, 2016, **28**, 1348–1354.

18 A. H. Slavney, T. Hu, A. M. Lindenberg and H. I. Karunadasa, *J. Am. Chem. Soc.*, 2016, **138**, 2138–2141.
19 G. E. Eperon, G. M. Paterno, R. J. Sutton, A. Zampetti, A. A. Haghighirad, F. Cacialli and H. J. Snaith, *J. Mater. Chem. A*, 2015, **3**, 19688–19695.
20 G. Kieslich, S. Sun and A. K. Cheetham, *Chem. Sci.*, 2014, **5**, 4712–4715.
21 R. D. Shannon, *Acta Crystallogr., Sect. A: Cryst. Phys., Diffr., Theor. Gen. Crystallogr.*, 1976, **32**, 751–767.
22 L. S. Chi, I. Swainson, L. Cranswick, J. H. Her, P. Stephens and O. Knop, *J. Solid State Chem.*, 2005, **178**, 1376–1385.
23 S. Sun, Y. Fang, G. Kieslich, T. J. White and A. K. Cheetham, *J. Mater. Chem. A*, 2015, **3**, 18450–18455.
24 T. D. Bennett, J.-C. Tan, S. A. Moggach, R. Galvelis, C. Mellot-Draznieks, B. A. Reisner, A. Thirumurugan, D. R. Allan and A. K. Cheetham, *Chem. – Eur. J.*, 2010, **16**, 10684–10690.
25 M. T. Weller, O. J. Weber, P. F. Henry, A. M. Di Pumpo and T. C. Hansen, *Chem. Commun.*, 2015, **51**, 4180–4183.
26 A. Filippetti and A. Mattoni, *Phys. Rev. B: Condens. Matter Mater. Phys.*, 2014, **89**, 125203.
27 Y. Le Page and P. Saxe, *Phys. Rev. B: Condens. Matter Mater. Phys.*, 2002, **65**, 104104.
28 J. F. Nye, *Physical properties of crystals: their representation by tensors and matrices*, Clarendon Press, Oxford, 1957.
29 M. A. Carpenter, *J. Phys.: Condens. Matter*, 2015, **27**, 263201.
30 R. E. A. McKnight, M. A. Carpenter, T. W. Darling, A. Buckley and P. A. Taylor, *Am. Mineral.*, 2007, **92**, 1665–1672.
31 L. J. Spalek, S. S. Saxena, C. Panagopoulos, T. Katsufuji, J. A. Schiemer and M. A. Carpenter, *Phys. Rev. B: Condens. Matter Mater. Phys.*, 2014, **90**, 054119.
32 M. A. Carpenter, A. Buckley, P. A. Taylor, R. E. A. McKnight and T. W. Darling, *J. Phys.: Condens. Matter*, 2010, **22**, 035406.
33 B.-W. Park, B. Philippe, T. Gustafsson, K. Sveinbjörnsson, A. Hagfeldt, E. M. J. Johansson and G. Boschloo, *Chem. Mater.*, 2014, **26**, 4466–4471.
34 G. Giorgi and K. Yamashita, *Chem. Lett.*, 2015, **44**, 826–828.